Journal of Materials Chemistry A

Accepted Manuscript

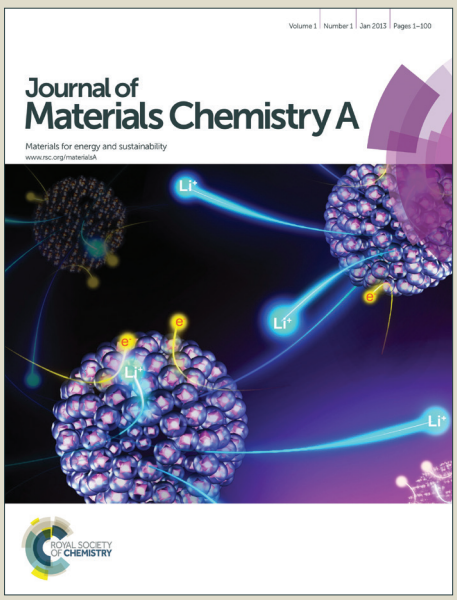

ROYAL SOCIETY OF CHEMISTRY

www.rsc.org/materialsA

Quasi-Graphene-Envelope Fe-doped Ni_2P Sandwiched Nanocomposites for Enhanced Water Splitting and Lithium Storage Performance

Yangyang Feng[a], Ya OuYang[a], Liang Peng[a], Huajun Qin[a]*, Hailiang Wang[b], Yu Wang[a]*

[a]*The State Key Laboratory of Mechanical Transmissions and School of Chemistry and Chemical Engineering, Chongqing University, Chongqing 400044, China;* [b]*Department of Chmistry, Yale University, 520 West Campus Drive, Energy Sciences Center 1, West Haven, CT06516*

*Email: wangy@cqu.edu.cn ; hjqiu@cqu.edu.cn

Key Words : Ni_2P, Graphene, water splitting, lithium storage, composite

Abstract

Developing advanced graphene-based composites is significant for the development of renewable green energy technology. Herein, we report a sandwich-like graphene-based composite (i.e., Fe-doped Ni_2P nanoparticles encapsulated by graphene-like envelope), which is synthesized by first polymerization of glucose (as a green carbon source) on the Fe-doped $NiNH_4PO_4{\cdot}H_2O$ nanosheet surface followed by high temperature annealing. The annealing process will crystalize the coated polymer into multi-layer graphene, as the same time, the Fe-doped precursor is decomposed into Fe-doped Ni_2P ((Fe)Ni_2P) nanoparticles encapsulated by the graphene envelope ((Fe)Ni_2P/graphene). When evaluated as a water splitting catalyst in acidic solutions, the graphene-encapsulated Fe-doped Ni_2P exhibits a low over-potential (~50 mV) and a small Tafel slop (~45 mV/decade) in 0.5 M H_2SO_4 solution. More importantly, the (Fe)Ni_2P/graphene composite shows an excellent stability in acid solutions in contrast to conventional Ni-based catalysts. On the other hand, owing to the structure advantage (i.e., efficient inner volume space for the nanoparticle expansion, high porosity for the electrolyte diffusion and high conductivity), the (Fe)Ni_2P/graphene nanocomposite exhibits a high specific capacity of 642 mAh g^{-1} at 0.2 C and excellent cycling stability (93% retained after 200 cycles).

Introduction

Hydrogen is being vigorously pursued as a future energy carrier in the transition from the current hydrocarbon economy.[1] In particular, sustainable hydrogen production from water splitting has attracted growing attention.[2] Currently, the state-of-the-art HER electrocatalysts are platinum or platinum-based materials, but the scarcity and high cost of platinum limit their practical applications. To search for non-precious electrocatalysts, recently, nanostructured MoS_2 attracted much attention due to its high HER activity and good stability in acidic solutions.[3] In alkaline solutions, the first-row metal nickel has been considered as one of the best candidates for HER.[4-7] Especially, the modification of the electronic structure of Ni by alloying with other components such as Mo, Co, Fe, etc. has been demonstrated to be good strategies to enhance the catalytic activity of Ni.[8-11] However, these Ni-based catalysts are not stable in acidic solutions, in which proton exchange membrane-based electrolysis occurs. To improve the stability of Ni-based catalysts in acidic solutions, the synthesis of Ni_2P[12] and Ni−Mo−N[13] nanoparticles has been pursued. Particularly, the P-based compounds attracted much research interest due to their high activity and stability in acidic solutions. For example, Ni_2P, CoP, and FeP nanoparticles have been successfully synthesized.[12, 14-17] Considering the modification effect on the electronic structure and possibly enhanced catalytic activity, the synthesis of Fe (or Co)-doped Ni_2P is very desirable. However, according to our knowledge, research in this direction has been rarely reported.

Graphene, a two-dimensional single-layer sheet of graphite with p-electrons fully delocalized on the graphitic plane, has attracted great attention due to its unique physicochemical properties, such as high surface area, high conductivity and strong mechanical strength.[18-21] Graphene has been exploited as a promising material for electrocatalyst support.[22-24] Meanwhile, it is found that there is strong electrical coupling effect between the graphene network and the supported electrocatalysts, which can remarkably enhance the catalytic properties.[22] Usually, the graphene-based composites are prepared by simple deposition or adsorption of nanocatalysts on graphene layer surface.[25-28] Due to the one-side attachment and weak interaction, the functional nanoparticles may be easily peeled off from the graphene surface during long-term electrochemical reactions. To solve this problem, the incorporation of

nanocatalysts inside two closely attached graphene layers would be a better strategy to enhance the stability of graphene-based composite materials.[29, 30] For example, Wang et al., fabricated a graphene-SnO_2 sandwich paper by using 7, 7, 8, 8-tetracyanoquinodimethane anion as both separator for graphene and complexing agent for Sn^{2+}.[31] Similarly, graphene-coated other nanostructures (such as Co_3O_4 nanospheres) have also been synthesized by using the electrostatic interaction between graphene oxides and the nanomaterials, followed by a reduction process.[32] However, the fabrication of this kind of sandwich-like graphene-based composites is very challenging.

In this contribution, we design a simple hydrothermal strategy combined with high temperature annealing to fabricate Fe-doped Ni_2P ((Fe)Ni_2P) nanoparticles encapsulated in graphene-like carbon envelope ((Fe)Ni_2P/graphene). Importantly, the (Fe)Ni_2P/graphene composite exhibits significantly enhanced catalytic activity for HER in acidic solutions compared with both Ni_2P/graphene and pure Ni_2P nanoparticles. Besides, owing to the high conductivity and efficient inner space provided by the double layer graphene-like envelope, the (Fe)Ni_2P/graphene also shows a very high specific capacity and charge/discharge stability in Lithium ion batteries (LIBs).

Results and discussions

The fabrication process of the graphene-encapsulated (Fe)Ni_2P composite is shown in Scheme 1. First, pure $NiNH_4PO_4{\cdot}H_2O$ nanosheets were synthesized by a hydrothermal method. The $NiNH_4PO_4{\cdot}H_2O$ nanosheets were then immersed in a $FeCl_2$ aqueous solution to prepare the Fe-doped $NiNH_4PO_4{\cdot}H_2O$ by an ion diffusion-exchange process. Due to the rich –OH group on the nanosheets surface, a second step hydrothermal process was then carried out to prepare the polymer-coated nanosheets using glucose as a green carbon source. In the last step, the polymerized glucose-coated Fe-doped $NiNH_4PO_4{\cdot}H_2O$ nanosheets were annealed in H_2 atmosphere at 680 °C. The annealing process would crystalize the carbon coating into

graphene-like carbon sheets and also decompose the Fe-doped $NiNH_4PO_4 \cdot H_2O$ nanosheets into Fe-doped Ni_2P nanoparticles, forming a sandwich-like composite.

XRD pattern in Fig. 1a shows that the synthesized precursor is pure $NiNH_4PO_4 \cdot H_2O$ with good crystallinity according to the sharpness of peaks from 5 to 90 degrees (JCPDS No.50-0425). SEM image reveals that the precursor possesses thin sheet-like morphology with a width of over 10 μm and thickness of around 40 nm (Fig. 1b, Fig. S1, Supporting Information). The thin sheet property is further demonstrated by the TEM in Fig. 1c. HRTEM image shows the single crystalline property of the precursor with 0.88 nm of interplanar distance from (010) crystal plane (inset in Fig. 1c). In order to prepare the (Fe)Ni_2P, the precursor was then mixed with 1 M $FeCl_2$ aqueous solution to obtain the Fe-doped $NiNH_4PO_4 \cdot H_2O$ by an ion diffusion-exchange process. Due to the similar atomic size of Fe and Ni, it is observed from the XRD pattern that the doping of Fe does not affect the crystal structure of the $NiNH_4PO_4 \cdot H_2O$. However, the doping of Fe in the precursor induces a remarkable color change as shown in Fig. 1d.

After polymerization with glucose and annealing, the sandwiched structure can be uniformly fabricated in a large scale (Fig. S2, Supporting Information). The enlarged SEM image shows that the thin sheet morphology of the precursor is well inherited by the crystallized thin carbon sheet (Fig. 2a). At the same time, the Fe-doped $NiNH_4PO_4 \cdot H_2O$ is decomposed into (Fe)Ni_2P nanoparticles with a diameter of ~10 nm encapsulated inside the graphene-like envelope. Composition analysis by energy dispersive X-ray spectroscopy (EDS) in Fig. 2b verifies that the final product is composed of C, P, Fe and Ni (The signal of Si is from the Si-based substrate used). The atomic ratio between Ni and P is around 2, suggesting the formed compound is Ni_2P and doping amount of Fe is ~6.3 at.%. To further clarify the elemental distribution of the final sandwich-like composite, selected area elemental mapping is carried out. As shown in Fig. 3, Ni, Fe and P are homogeneously distributed in the encapsulated nanoparticles, confirming that Fe is successfully doped into Ni_2P via the ion diffusion-exchange process followed by high temperature annealing.

XRD analysis further confirms the phase-pure properties of the Fe-doped Ni_2P nanoparticles (Fig. 4a). No other Fe-based diffraction peaks are observed, indicating that Fe atoms should be distributed in the atomic structure of Ni_2P. Furthermore, a small and weak peak around 26.6° can be also find in this pattern, indexed to graphite (JCPDS No. 75-2078), which affirms that we have successfully synthesized graphene under typical condition by low-cost and environmentally friendly glucose. The (Fe)Ni_2P/graphene composite is further characterized by transmission electron microscopy (TEM). The low-magnification bright-field TEM image (Fig. 4b) clearly shows that the formed (Fe)Ni_2P nanoparticles are uniformly distributed in the graphene-like envelope, consistent with the SEM observations. High-resolution TEM (HRTEM) in Fig. 4c reveals that the encapsulated (Fe)Ni_2P nanoparticles are well-crystallized with dominated (111) plane, which may be inherited from the dominated (010) plane of the precursor. Through the HERTM image (Fig. S3, Supporting Information) of the thin carbon film, hexagonal lattice can be observed, confirming that the thin carbon film is crystallized by the high temperature annealing. The graphitization degree of the graphene envelope is further characterized by Raman spectroscopy. It is known that the D band peak indicates the disordered graphitic crystal stacking while G band increases with the number of the graphene layers.[30, 33, 34] The degree of crystallinity can be relatively determined by the I_D/I_G ratio. A lower I_D/I_G ratio corresponds to a high crystallization degree. As shown in Fig. 5a, the I_D/I_G ratio of the graphene envelop is near 1, which is higher than that of reduced graphene oxides (r-GO), indicating the good crystallization of the carbon sheets by annealing at an appropriate temperature. The Brunauer–Emmett–Teller (BET) surface area of the composite is estimated as 364.7 $m^2 g^{-1}$ and pore diameter is around 2 nm with the Barrett-Joyner-Hallender (BJH) method (Fig. 5b and c). The result indicates that the graphene-based composite possesses many small pores which would allow the free diffusion of electrolyte during electrochemical reactions.

The catalytic performance of the encapsulated (Fe)Ni_2P in graphene composite is then evaluated in 0.5 M H_2SO_4 solution using a typical three-electrode setup. Fig. 6a shows the polarization curves (current-potential plots) of the (Fe)Ni_2P/graphene with

those of the encapsulated Ni_2P in graphene, pure Ni_2P and Pt included for comparison. It is observed that the (Fe)Ni_2P/graphene nanocomposite shows a small overpotential (η) of ~50 mV for HER, beyond which the cathodic current rose rapidly. The Ni_2P/graphene composite also exhibits a similar small overpotential, however, at the same potential, the (Fe)Ni_2P/graphene composite clearly shows a larger current response, indicating the enhanced catalytic activity for HER owing to the Fe doping. The enhanced performance of the Ni_2P/graphene compared with that of pure Ni_2P, demonstrating the positive effect of the structure design (i.e., graphene envelope coating) on the catalytic activity. The over-potential of the (Fe)Ni_2P/graphene catalyst is also much lower than MoS_2/r-GO (~100 mV),[22] defect-rich MoS_2 nanosheets (~120 mV)[35] and chemically exfoliated WS_2 (80-100 mV)[36]. Quite recently, Yu and coworkers reported a Ni/NiO/$CoSe_2$ catalyst which exhibited a low over-potential of 30-50 mV in 0.5 M H_2SO_4 solution.[37] However, this Ni nanoparticle-based catalyst is not stable in acidic solutions. The linear portions of the Tafel plots are then fit to the Tafel equation (η= b log(j) + a, where j is the current density and b is the Tafel slope), yielding Tafel slopes of ~45 mV/decade for the (Fe)Ni_2P/graphene (Fig. 6b). This value is comparable to the lowest values (41 mV from graphene supported MoS_2) reported for nonprecious catalyst.[22, 35] Based on the amount of catalyst on the (Fe)Ni_2P/graphene electrode, the calculated turnover frequency (TOF) for the catalyst at η=0.3 V reaches ~0.8 s^{-1}, which is higher than the TOF of defect-rich MoS_2 nanosheet catalyst (0.72 s^{-1}),[35] indicating the high intrinsic catalytic activity.

To evaluate the long-term stability of the catalysts in acidic solutions, we then studied the catalysts at both constant current and CV cycling conditions. As shown in Fig. 6c, generating a constant current density of 20 mA cm^{-2}, the applied potential on the (Fe)Ni_2P/graphene composite is the lowest and almost constant for over 11 h (increased by 4.3%). Under the same conditions, the other two catalysts clearly required higher potentials and after 11 h, the potential increased by ~37% for the Ni_2P/graphene and ~66% for the pure Ni_2P. We also tested the durability of the (Fe)Ni_2P/graphene under continuous potential scanning condition. After 1000 cycles, the (Fe)Ni_2P/graphene catalyst only shows slight decrease (Fig. 6d). These results indicate that our encapsulated (Fe)Ni_2P nanocomposite can be used as a stable HER catalyst in acid environments. In addition, the (Fe)Ni_2P/graphene can also endure a big temperature variation in acidic solutions (Fig. S4, Supporting Information). It is

observed that the overpotential only increases slightly from 40 to 50 and 60 mV when the temperature decreases from 50 to 25 and 0 ^{o}C, respectively.

The high catalytic activity should originate from the uniformly distributed nanoscale (Fe)Ni_2P particles which provide rich active sites for the HER reaction. The Fe atomic doping clearly enhances the catalytic activity due to the modification effect on the atomic and electronic structure of Ni_2P. Additionally, both top and bottle graphene layers tightly coated on the surface of (Fe)Ni_2P nanoparticles can effectively prevent active nanoparticles from aggregation and peeling-off during long-time electrochemical reactions, thereby leading to superior cyclic stability. On the other hand, the porous structure derived from a large amount of substance loss would guarantee efficient diffusion pathways for both H^+ ions and electrons, inducing a possible synergistic effect. More importantly, the porous graphene envelope clearly plays a key role for stabilizing the (Fe)Ni_2P by the strong interaction, which allows the Ni-based catalyst to work stably in the acidic solutions. The stabilizing effects of graphene on other catalyst have also been reported elsewhere.[38]

The (Fe)Ni_2P/graphene composite is also evaluated as an anode for LIBs. Fig. 7a shows the CV curves from 0 to 3 V vs Li/Li^+. It is observed that from the second cycles, the CV curves become stable, suggesting the reversible Li storage process. According to previous investigations, the electrochemical Li storage mechanism for Ni_2P is believed to originate from an alloying/dealloying process, similar to Si, Sn, Ge, etc., which can be written as follows: $Ni_2P + 3Li^+ + 3e^- \leftrightarrow Li_3P + 2Ni$.[14, 32] Fig. 7b shows the galvanostatic discharge-charge curves of the (Fe)Ni_2P/graphene at 0.2 C between 0.01 and 3.0 V vs Li/Li^+. It is observed that the as-synthesized (Fe)Ni_2P/graphene nanocomposite exhibits a high initial discharge capacity of ~1000 mAh g^{-1}, which is significantly higher than the theoretical capacity of Ni_2P (542 mAh g^{-1}). The excess discharge capacity could be associated with the initial formation of the solid-electrolyte-interface (SEI) layer resulted from electrolyte degradation, which is a common phenomenon and also observed in many other anode materials. Staring from the second cycles, the capacity decreases to ~642 mAh g^{-1} and the charge/discharge process becomes very stable after even 200 cycles (93% of the capacity from the second cycle retained) with high Coulombic efficiency (~95%), indicating the high specific capacitance and excellent cycling stability of the (Fe)Ni_2P/graphene composite (Fig. 7c). The stabilized specific capacity (after second

cycle) is also considerably higher than most reported values on Ni_2P-based anode materials such as carbon-coated Ni_2P nanoparticles[39] (435 mAh g^{-1} at 0.1 C) and Ni_2P nanowires[40] (434 mA h g^{-1} at 0.1 C). To further evaluate its cycling stability and rate performance, continuous increase in current density from 0.2 C to 20 C was carried out (Fig. 7d). It is observed that the capacity decreases with the increase of current density. When 20 C is applied, the capacity is still 350 mAh g^{-1} (which is ~52% of the capacity at 0.2 C), indicating the good rate performance. Moreover, when cycled back to 0.2 C, the capacity recovered can reach ~624 mAh g^{-1}, which further demonstrates the excellent cycling stability of the designed nanocomposite. The enhanced Li storage performance is clearly resulted from the unique structure designed. Firstly, the graphene-like envelope-shaped carbon coating can not only enhance the electronic conductivity (as shown in AC impedance spectrum in Fig. S5, the graphene-encapsulated samples exhibit remarkably low charge-transfer resistance) but also prevent the encapsulated (Fe)Ni_2P nanoparticles from detachment, aggregation, and pulverization. The carbon content of the final samples is calculated as 6.1 wt% (shown in Experimental Section), which can hardly lower the theoretical capacity of active materials, on the contrary, enhance the electrochemical performances due to their synergic effect. Secondly, the efficient inner space would allow the volume expansion of the functional nanoparticles while retaining the high conductivity. Thirdly, the nanoporosity is highly favorable for the free diffusion of electrolyte and the exchange rate of lithium ions. To further affirm the structural passability, we revisit the status of the sandwiched (Fe)Ni_2P/graphene after 200 cycles of charge-discharge process. As expected, the sandwiched is well-maintained even for a long time running and the crystal lattice of (Fe)Ni_2P can be distinctly revealed (Fig. S6, supporting information), which significantly clarify the morphology integrity of the sandwich-like structure. Our experimental results clearly reveal the synergic effects of this kind of architecture design in both HER and LIBs and this desiging/fabricating strategy is expected to be realized on other systems.

Conclusions

Uniform Fe-doped Ni_2P nanoparticles encapsulated in graphene-like envelope were successfully synthesized by first polymerization of glucose on Fe-doped

$NiNH_4PO_4 \cdot H_2O$ nanosheets and followed by high temperature annealing. This designed graphene-based composite possess many unique structure properties such as intimate contact between the encapsulated nanoparticles and two graphene sheets, high nanoporosity, large specific surface area and efficient inner void space. Owing to the unique nanostructure, the synthesized (Fe)Ni_2P/graphene composite exhibited high and stable performance when used as water splitting electrocatalysis and anode materials in LIBs. We believe that this work presents a new strategy for designing advanced graphene-encapsulated functional nanocomposite materials.

Experimental section

Preparation of $NiNH_4PO_4 \cdot H_2O$ nanosheets

In a typical synthesis of $NiNH_4PO_4 \cdot H_2O$, concentrated $NH_3 \cdot H_2O$ (3 mL), ethylene glycol (17.5 mL), 1 mL $Ni(NO_3)_2$ aqueous solution (1 M), 5 mL NaH_2PO_4 aqueous solution (1 M) and 1 mL Na_2CO_3 aqueous solution (1 M) were mixed step-by-step under strong stirring. The mixed solution was then transferred into a Teflon-lined stainless-steel autoclave and kept at 170 ^oC for 24 h. After the autoclave was cooled naturally to room temperature, the yellow precipitate at the bottom were collected and washed at least three cycles by deionized water and one cycle by pure ethanol. The as-synthesized samples were then dried in a normal oven at 60 ^oC overnight to remove the absorbed water for the subsequent characterizations and further treatment.

Preparation of Fe-doped $NiNH_4PO_4 \cdot H_2O$ nanosheets

The as-prepared $NiNH_4PO_4 \cdot H_2O$ nanosheets (250 mg) were ultrasonically mixed with 40 mL $FeCl_2$ aqueous solution (1 M) to form a homogeneous solution. The mixture was standing for 1 h at room temperature until the color of the nanosheets slowly turned to yellow-green. Finally, the samples were washed for three cycles by deionized water and one cycle by ethanol, and then dried in a normal oven at 60 ^oC.

Preparation of the Fe-doped Ni_2P nanoparticles encapsulated in graphene-like envelope

Fe-doped $NiNH_4PO_4 \cdot H_2O$ nanosheets were mixed with 5 mL glucose aqueous solution (1 M) and 25 mL deionized water to form a homogeneous solution by ultrasonication for 10 min. The solution was poured into a 50 mL Teflon-lined autoclave and heated at 180 ^oC for 8 h. After that, the samples were washed (three cycles by deionized water and one cycle by ethanol), and then dried in air at 60 ^oC for 24 h to remove the residual water and ethanol. Afterwards, the dried samples were loaded into the tube furnace and calcined at 680 ^oC for 200 min in H_2 atmosphere.

Carbon content of sandwiched (Fe)Ni_2P / graphene

200mg final samples were dissolved in concentrated hydrochloric acid (10 M) under vigorous stirring. Standing for almost 2 days, the final samples floated on the

liquid level. Afterwards, the samples were washed using centrifugation with three cycles of deionized water and one cycle of ethanol, and then dried in air at 60 ^{o}C for 24 h to remove the residual water and ethanol. The carbon content of sandwiched (Fe)Ni_2P / graphene was then calculated using the formula:

$$C\%=W(C)/W((Fe)Ni_2P\ /C)\times 100\%$$

Where W(C) and W ((Fe)Ni_2P /C) were the weight of carbon and (Fe)Ni_2P/graphene, respectively.

Material characterization

The synthesized materials are characterized on a transmission electron microscope (TEM, Philips, Tecnai, F30), field-emission scanning electron microscope (SEM, JSM-7800F) equipped with an energy dispersive spectrometer (EDS) analyzer, X-ray diffractometer with Cu Kα radiation (XRD, Bruker D8 Advance), BET surface-area and pore-size analyzer (Quantachrome Autosorb-6B), and Raman Microscope (RENISHAW Invia, UK, voltage (AC) 100-240V, Power 150W).

Electrochemical measurements

Hydrogen evolution reaction was performed on a CHI660E electrochemical workstation using a three-electrode setup, including a modified glassy carbon electrode (GCE, 3 mm in diameter) as working electrode, a saturated calomel electrode (SCE) as reference electrode, and a Pt foil as counter electrode. The catalyst suspension of both our final materials and Pt/C (Aldrich) was made by mixing 3 mg catalyst, 100 μL Nafion solution (0.5 wt%) and 300 μL ethanol solvent under ultrasonication treatment for 20 min. The working electrode was made by dropping 4 μL suspension on the GCE (~loading: 0.36 mg cm^{-2}) and dried at room temperature. Linear sweep voltammetry (LSV) was performed in 0.5 M H_2SO_4 solution at a scan rate of 5 mV s^{-1}. Durability test was done by cyclic voltammetry (CV) cycling from

-0.5 to 0 V at 50 mV s^{-1}. All the potentials appeared in the water splitting section were vs. the reversible hydrogen electrode (RHE) according the equation: E (RHE) = E (SCE) + 0.279 V in 0.5 M H_2SO_4 solution.

For lithium-ion battery test, a slurry was made by mixing 75 wt.% (Fe)Ni_2P/graphene composite, 15 wt.% carbon black and 10 wt.% polyvinylidene fluoride (PVDF) with the help of N-methyl pyrrolidinone (NMP). The slurry was then magnetically stirred for 1 day to make a homogeneous mixture. The homogeneous slurry was spread on a piece of nickel foam (12 mm in diameter) to make the electrode. The mass loading of the electrode material is about 2.2 mg/cm^2. After drying at 90 ^oC for 24 h in vacuum, the batteries were assembled in an argon-filled glove box under a pressure of 20 Mpa with metallic lithium foil (99.9%, Aldrich) as the counter electrode, 1 M $LiPF_6$ in ethylene carbonate (EC)/dimethyl carbonate (DME) (volume ratio: 1 : 1) as the electrolyte, and a polypropylene (PP) microporous film (Cellgard2400) as the separator. The galvanostatic charge/discharge tests were carried out on a LAND battery program-control test system at rates of 0.2-10 C (1 C = 542 mA g^{-1}) between the voltage range of 0.01–3.0 V (versus Li/Li^+) at room temperature. Cyclic voltammetry (CV) tests were performed on a CHI660E electrochemical work station with a scan rate of 0.5 mV s^{-1}.

Acknowledgements

Financial support is from Thousand Young Talents Program of the Chinese Central Government (No. 0220002102003), National Natural Science Foundation of China (NSFC, No. 21373280, 21403019), Beijing National Laboratory for Molecular Sciences (BNLMS) and Hundred Talents Program at Chongqing University (No. 0903005203205).

Reference

1. M. S. Dresselhaus and I. L. Thomas, *Nature*, 2001, **414**, 332-337.
2. M. G. Walter, E. L. Warren, J. R. McKone, S. W. Boettcher, Q. Mi, E. A. Santori and N. S. Lewis, *Chem. Rev.*, 2010, **110**, 6446-6473.
3. T. F. Jaramillo, K. P. Jorgensen, J. Bonde, J. H. Nielsen, S. Horch and I. Chorkendorff, *Science*, 2007, **317**, 100-102.
4. Y. Choquette, L. Brossard, A. Lasia and H. Ménard, *Electrochim. Acta*, 1990, **35**, 1251-1256.
5. N. Danilovic, R. Subbaraman, D. Strmcnik, K. C. Chang, A. P. Paulikas, V. R. Stamenkovic and N. M. Markovic, *Angew. Chem. Int. Edit.*, 2012, **51**, 12495-12498.
6. R. Subbaraman, D. Tripkovic, K. C. Chang, D. Strmcnik, A. P. Paulikas, P. Hirunsit, M. Chan, J. Greeley, V. Stamenkovic and N. M. Markovic, *Nat. Mater.*, 2012, **11**, 550-557.
7. R. Subbaraman, D. Tripkovic, D. Strmcnik, K. C. Chang, M. Uchimura, A. P. Paulikas, V. Stamenkovic and N. M. Markovic, *Science*, 2011, **334**, 1256-1260.
8. L. Xiao, S. Zhang, J. Pan, C. X. Yang, M. L. He, L. Zhuang and J. T. Lu, *Energy Environ. Sci.*, 2012, **5**, 7869-7871.
9. J. R. McKone, B. F. Sadtler, C. A. Werlang, N. S. Lewis and H. B. Gray, *ACS Catal.*, 2012, **3**, 166-169.
10. F. Rosalbino, S. Delsante, G. Borzone and E. Angelini, *Int. J. Hydrogen Energy*, 2008, **33**, 6696-6703.
11. N. V. Krstajić, V. D. Jović, L. Gajić-Krstajić, B. M. Jović, A. L. Antozzi and G. N. Martelli, *Int. J. Hydrogen Energy*, 2008, **33**, 3676-3687.
12. E. J. Popczun, J. R. McKone, C. G. Read, A. J. Biacchi, A. M. Wiltrout, N. S. Lewis and R. E. Schaak, *J. Am. Chem. Soc.*, 2013, **135**, 9267-9270.
13. W. F. Chen, K. Sasaki, C. Ma, A. I. Frenkel, N. Marinkovic, J. T. Muckerman, Y. M. Zhu and R. R. Adzic, *Angew. Chem. Int. Edit.*, 2012, **51**, 6131-6135.
14. G. Li, L. Feng, J. Chang, B. Wickman, H. Grönbeck, C. Liu and W. Xing, *ChemSusChem*, 2014, n/a-n/a.
15. Q. Liu, J. Tian, W. Cui, P. Jiang, N. Cheng, A. M. Asiri and X. Sun, *Angew. Chem.*, 2014, **126**, 6828-6832.
16. E. J. Popczun, C. G. Read, C. W. Roske, N. S. Lewis and R. E. Schaak, *Angew. Chem. Int. Ed.*, 2014, **53**, 5427-5430.
17. P. Jiang, Q. Liu, Y. Liang, J. Tian, A. M. Asiri and X. Sun, *Angew. Chem.*, 2014, **126**, 13069-13073.
18. C. Lee, X. D. Wei, J. W. Kysar and J. Hone, *Science*, 2008, **321**, 385-388.
19. K. S. Novoselov, A. K. Geim, S. V. Morozov, D. Jiang, Y. Zhang, S. V. Dubonos, I. V. Grigorieva and A. A. Firsov, *Science*, 2004, **306**, 666-669.
20. Z. Jin, J. Yao, C. Kittrell and J. M. Tour, *ACS Nano*, 2011, **5**, 4112-4117.
21. K. Yan, L. Fu, H. Peng and Z. Liu, *Acc. Chem. Res.*, 2013, **46**, 2263-2274.
22. Y. G. Li, H. L. Wang, L. M. Xie, Y. Y. Liang, G. S. Hong and H. J. Dai, *J. Am. Chem. Soc.*, 2011, **133**, 7296-7299.
23. Y. Zhao, S. Chen, B. Sun, D. Su, X. Huang, H. Liu, Y. Yan, K. Sun and G. Wang, *Sci. Rep.*, 2015, **5**.
24. Y. Zhao, B. Sun, X. Huang, H. Liu, D. Su, K. Sun and G. Wang, *J. Mater. Chem. A*, 2015, **3**,

5402-5408.

25. Y. Lu, X. Wang, Y. Mai, J. Xiang, H. Zhang, L. Li, C. Gu, J. Tu and S. X. Mao, *J. Phys. Chem. C*, 2012, **116**, 22217-22225.
26. G. Zhou, D.-W. Wang, F. Li, L. Zhang, N. Li, Z.-S. Wu, L. Wen, G. Q. Lu and H.-M. Cheng, *Chem. Mater.*, 2010, **22**, 5306-5313.
27. S. Yang, X. Feng, S. Ivanovici and K. Müllen, *Angew. Chem. Int. Ed.*, 2010, **49**, 8408-8411.
28. S.-W. Kim, D.-H. Seo, H. Gwon, J. Kim and K. Kang, *Adv. Mater.*, 2010, **22**, 5260-5264.
29. Y. Wang, Y. Bai, X. Li, Y. Feng and H. Zhang, *Chem. Eur. J.*, 2013, **19**, 3340-3347.
30. H. Zhang, Y. Bai, Y. Feng, X. Li and Y. Wang, *Nanoscale*, 2013, **5**, 2243-2248.
31. X. Wang, X. Cao, L. Bourgeois, H. Guan, S. Chen, Y. Zhong, D.-M. Tang, H. Li, T. Zhai, L. Li, Y. Bando and D. Golberg, *Adv. Funct. Mater.*, 2012, **22**, 2682-2690.
32. H. Sun, X. Sun, T. Hu, M. Yu, F. Lu and J. Lian, *J. Phys. Chem. C*, 2014, **118**, 2263-2272.
33. J. Ha, S. K. Park, S. H. Yu, A. Jin, B. Jang, S. Bong, I. Kim, Y. E. Sung and Y. Piao, *Nanoscale*, 2013, **5**, 8647-8655.
34. E. Flahaut, F. Agnoli, J. Sloan, C. O'Connor and M. L. H. Green, *Chem. Mater.*, 2002, **14**, 2553-2558.
35. J. Xie, H. Zhang, S. Li, R. Wang, X. Sun, M. Zhou, J. Zhou, X. W. Lou and Y. Xie, *Adv. Mater.*, 2013, **25**, 5807-5813.
36. D. Voiry, H. Yamaguchi, J. W. Li, R. Silva, D. C. B. Alves, T. Fujita, M. W. Chen, T. Asefa, V. B. Shenoy, G. Eda and M. Chhowalla, *Nat. Mater.*, 2013, **12**, 850-855.
37. Y. F. Xu, M. R. Gao, Y. R. Zheng, J. Jiang and S. H. Yu, *Angew. Chem. Int. Edit.*, 2013, **52**, 8546-8550.
38. H. L. Wang and H. J. Dai, *Chem. Soc. Rev.*, 2013, **42**, 3088-3113.
39. Y. Lu, J.-p. Tu, C.-d. Gu, X.-l. Wang and S. X. Mao, *J. Mater. Chem.*, 2011, **21**, 17988-17997.
40. Y. Lu, J. P. Tu, Q. Q. Xiong, Y. Q. Qiao, X. L. Wang, C. D. Gu and S. X. Mao, *RSC Adv.*, 2012, **2**, 3430-3436.

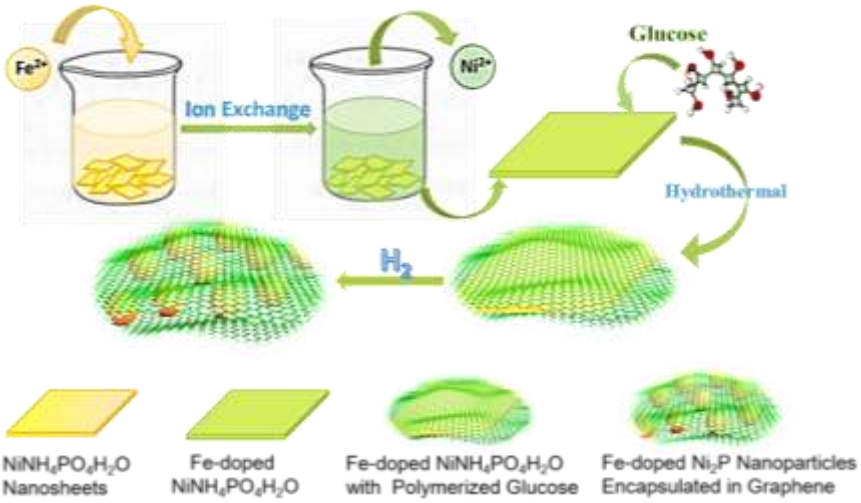

Scheme 1. Schematic explanation of the synthesis process of the (Fe)Ni_2P/graphene composite.

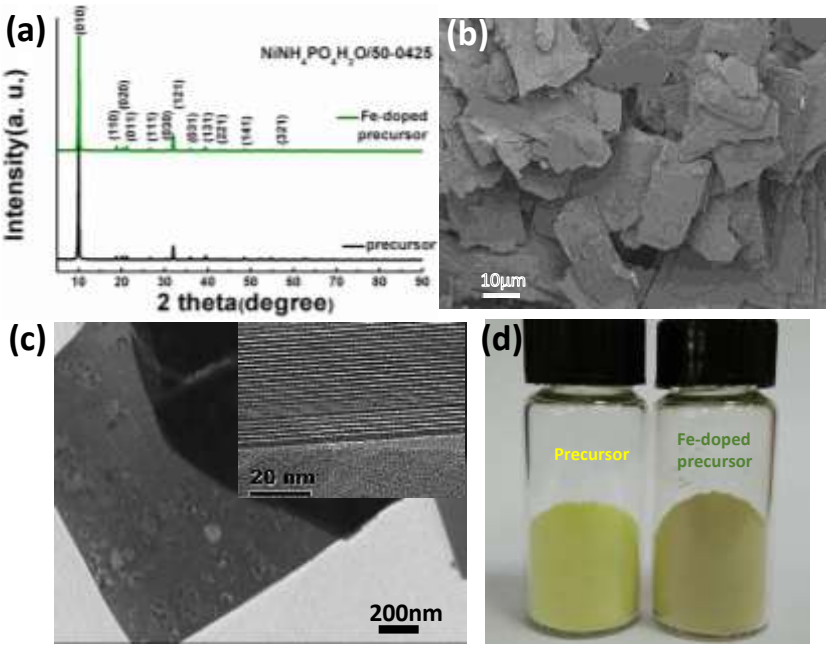

Figure 1. (a) XRD patterns of the precursors before and after Fe doping. (b) SEM image of the $NiNH_4PO_4 \cdot H_2O$ precursor. (c) TEM and HRTEM (inset) images of the precursor nanosheets. (d) Photos of the precursor before and after doping with Fe.

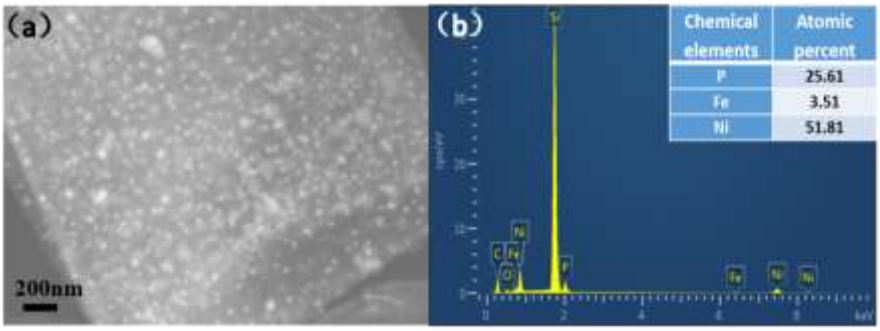

Figure 2. (a) SEM image, (b) EDS spectrum of the (Fe)Ni_2P/graphene composite.

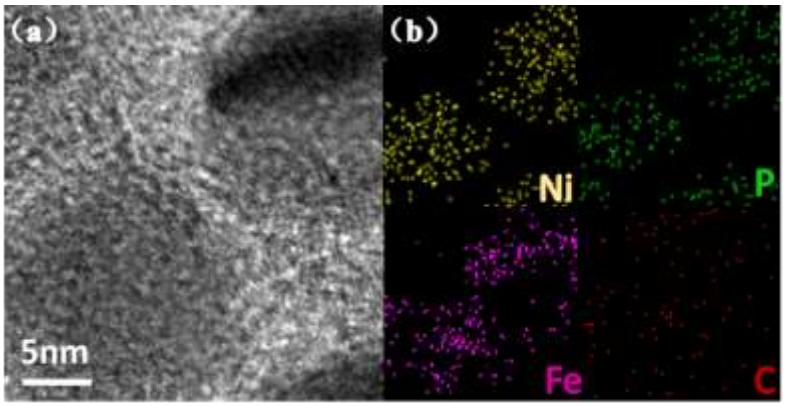

Figure 3. Elemental mapping of the (Fe)Ni_2P/graphene composite via EDS. (a) is the TEM image and (b) is the distribution of Ni, Fe, P and C.

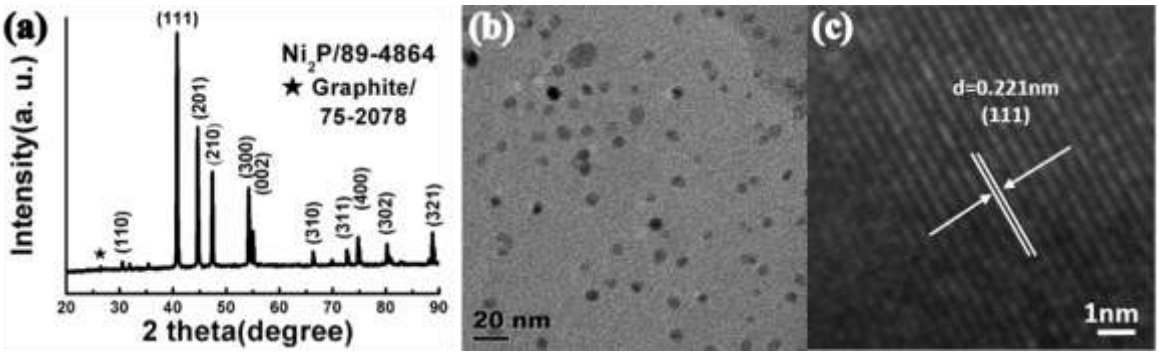

Figure 4. (a) XRD pattern, (b) TEM and (c) HRTEM images of the (Fe)Ni_2P/graphene composite.

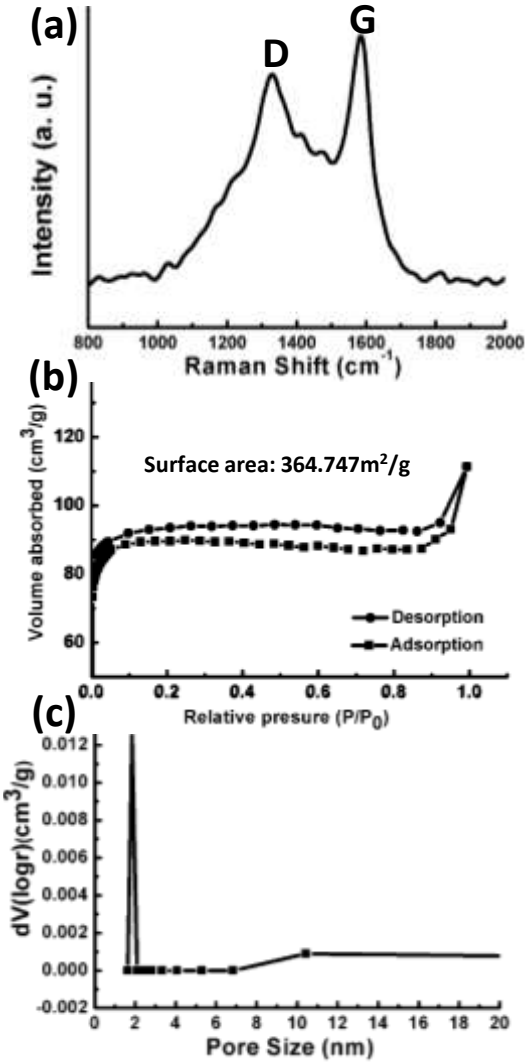

Figure 5. (a) Raman spectrum, (b) nitrogen adsorption/desorption curve and (c) the pore size distribution of the (Fe)Ni_2P/graphene composite.

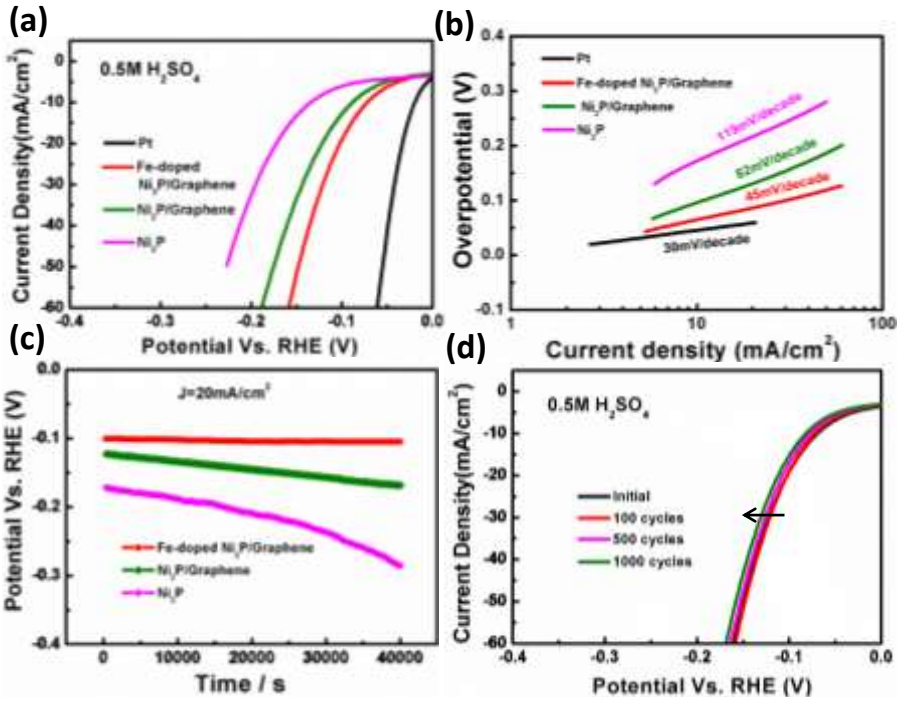

Figure 6. (a) Polarization curves of the graphene-encapsulated composites along with pure Ni_2P nanoparticles and Pt for comparison (0.5 M H_2SO_4, scan rate: 5 mV s^{-1}). (b) Tafel curves obtained from the polarization curves. (c) Potential change of the catalysts when generating a constant current density of 20 mA cm^{-2}. (d) Durability test for the (Fe)Ni_2P/graphene composite after 1000 cycles.

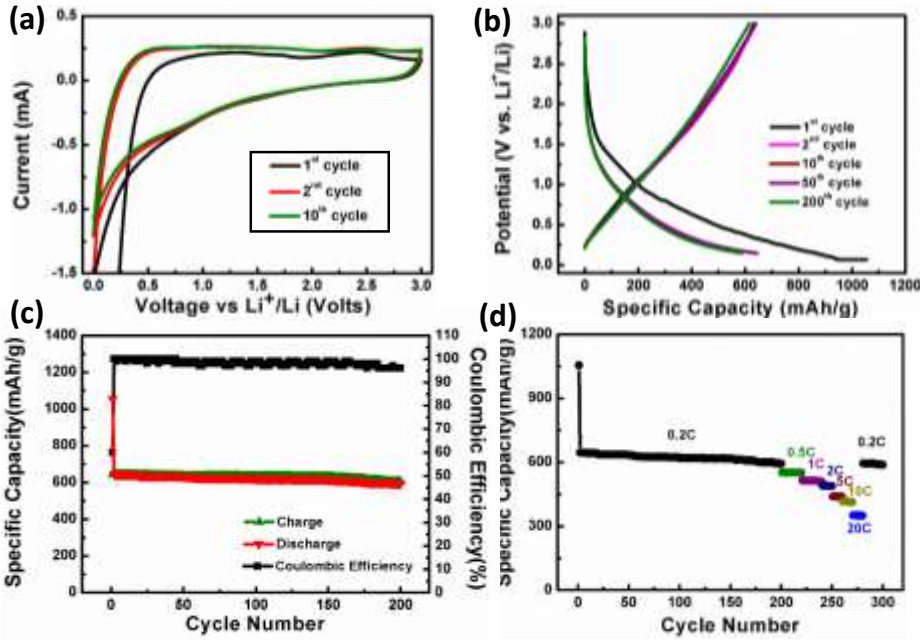

Figure 7. Electrochemical performance of the (Fe)Ni_2P/graphene composite. (a) CV ; (b) galvanostatic charge/discharge curves at 0.2 C; (c) cycling performance and coulombic efficiency at 0.2 C and (d) rate performance of the (Fe)Ni_2P/graphene composite.

Table of Contents Entry

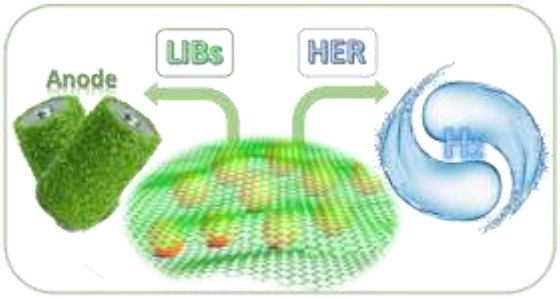

We report a sandwich-like graphene-based composite, which exhibits enhanced performance for both electrochemical water splitting and lithium ion batteries.